Growth, corrosion, and wear study of nanocomposite PEO coating in electrolyte containing nickel sulfate

Ali Abolhassani, Mahmood Aliofkhazraei[*], Seyed Saeed Farhadi, Alireza Sabour

Rouhaghdam and Masoud Asgari

Department of Materials Science, Faculty of Engineering, Tarbiat Modares University, Tehran, Iran, P.O.Box: 14115-143.

[*] *Corresponding author Email: maliofkh@gmail.com, khazraei@modares.ac.ir, Tel.: +98-912-6905626, Fax: +98-21-82884969*

Abstract

Plasma electrolytic oxidation (PEO) was performed on a 1010 Aluminum alloy. To achieve the nanocomposite structure, Si_3N_4 nanoparticles were added into the electrolyte. In an alkaline aqueous suspension (silicate-based), the effect of adding $NiSO_4$ on the applied voltage, microstructure, composition, wear, and corrosion resistance of PEO coatings was investigated using Scanning Electron Microscopy (SEM), elemental analysis with Energy Dispersive Spectroscopy (EDS), X-Ray Diffraction (XRD), cyclic polarization test, and pin-on-disk wear test. The results showed that adding nickel sulfate ($NiSO_4$) and infiltration of its constituents into coatings lead to a more favored corrosion behavior. Moreover, in the case of best sample, anodic current at the highest applied potential condition during the cyclic polarization test indicated a drop within two decades. Moreover, coefficient of friction decreased almost by half.

Keywords: *aluminum, corrosion, electrolyte, nanocomposite, nickel sulfate, plasma electrolytic oxidation.*

1. Introduction

The ever-increasing demand for lighter, recyclable, and more resistant alloys as well as technical and economic considerations has recently led to wide use of aluminum and its alloys. Because of their low density, relatively suitable physical and chemical performance, resistivity to high weight, and abundant reserves, aluminum alloys are among the most attractive materials for researchers and industries. Currently, aluminum is the second most commonly used metal after steel. Furthermore, aluminum has many applications in aerospace, cars, high-speed trains, etc. Nevertheless, due to the low hardness of aluminum, wear and erosion decreases the lifetime of the pieces build using it. Thus, for applications that require high load-bearing capacity, aluminum is not so favored. Among other methods applied for improving aluminum alloys, one can name plating, conversion coating, anodizing, polymeric coating, physical vapor deposition (PVD), etc. [1-4].

Anodizing is a cheap and traditional method to improve the performance of aluminum. However, due to its low thickness and porosity, it does not provide adequate corrosion resistance [5]. Considering the excellent properties of alumina and the need for achieving high corrosion and wear resistance, coating methods able to make a

layer of alumina on substrate are prioritized. Excellent properties of alumina depend on its substrate and phase. Alumina has many different crystalline phases such as the κ, θ, δ, χ, η, γ, ρ, and β phases. In this regard, α-Al_2O_3 is the most stable and hardest of these phases [6]. One method to produce these coatings is plasma electrolytic oxidation (PEO).

PEO, also called Micro-arc oxidation (MAO), spark anodizing (SO), and micro-plasma oxidation (MPO), is a promising novel process to form hard and thick Ceramic-like coatings on valve metals (Al, Mg, Ti, etc.) and their alloys [7-9]. PEO is a complex process combined with simultaneous partial processes, including oxide film formation, dissolution, and dielectric breakdown. Previous studies showed that coating presents an appropriate combination of corrosion, wear and mechanical resistance, surface tension, and suitable mechanical properties.

Such a process includes generating a large number of micro-arcs on the surface of the substrate at a high voltage for a short time, which makes the surface to be heated and cooled rapidly. The coating has a crystal structure and includes numerous discharge channels that their sizes depend on the reaction time of PEO. Coatings made of the PEO are generally porous. Big discharge channels are harmful for corrosion and wear resistance. The microstructure of PEO coatings is controlled by the chemical composition and concentration of the electrolyte, current density, mode of power supply, and the substrate composition. Certainly, chemical composition has the highest effect on the final properties of the PEO coatings. Therefore, changing the chemical composition of electrolyte, it would be possible to obtain a denser microstructure and better corrosion and wear properties [10-15].

Due to high impressibility of coating from the electrolyte, in this study, $NiSO_4$ was added to electrolyte to investigate its effect on coating properties. According to the extensive studies concerning organic additives, in this study, a mineral material was employed so that the effects of these materials be included as well. Moreover, $NiSO_4$, as an environmental advocate salt and corrosion resistance inducer, is one of the materials used in electrochemical coatings. $NiSO_4$ is dissolved in water easily and known as nickel ion source [16].

In addition, to increase corrosion and wear resistance of these coatings as well as producing nanocomposite structure, nanoparticles were employed. As previous studies showed, increasing the nanoparticles causes improvement of these properties [17, 18]. In this study, Si_3N_4 nano-powder was used to create a nanocomposite structure. The effect of adding $NiSO_4$ on the absorption of nanoparticles as well as corrosion and wear behavior of coatings was also investigated.

2. Materials and Methods

In this study, commercial 1010 aluminum foil with the size of 50×50 mm and thickness of 1 mm was used. Before the coating process, alkaline wash was performed in a 10 wt% NaOH solution. A 20KW homemade PEO device with DC current regime and the stainless steel cathode was used. Coating of the samples was performed as shown in Table 1. Effect of the applied current parameter was investigated. The electrolyte used in this system was a solution consisting of $Na_2SiO_3.5H_2O$ (8 gr/lit), KOH (1 gr/lit), and Si_3N_4 nanopowder (5 gr/lit) with the size of 37 nm. Using PHILIPS CM 200 TEM/STEM unit, the powder was investigated at a nonometric scale (Fig. 1). To observe the created nanocomposite structure, the TEM ((Zeiss-EM10C) apparatus was utilized. Coating time of all samples was 15 minutes. After PEO process, samples were washed with distilled water and then dried in air.

Table 1. Current density and concentration of additive utilized for coating the samples

sample	Current (mA/cm^2)	Concentration of additive (g/lit)
A-15-13	15	0.13
A-15-26	15	0.26
A-15-40	15	0.40
A-25-13	25	0.13
A-25-26	25	0.26
A-25-40	25	0.40
p-15	15	0
p-25	25	0
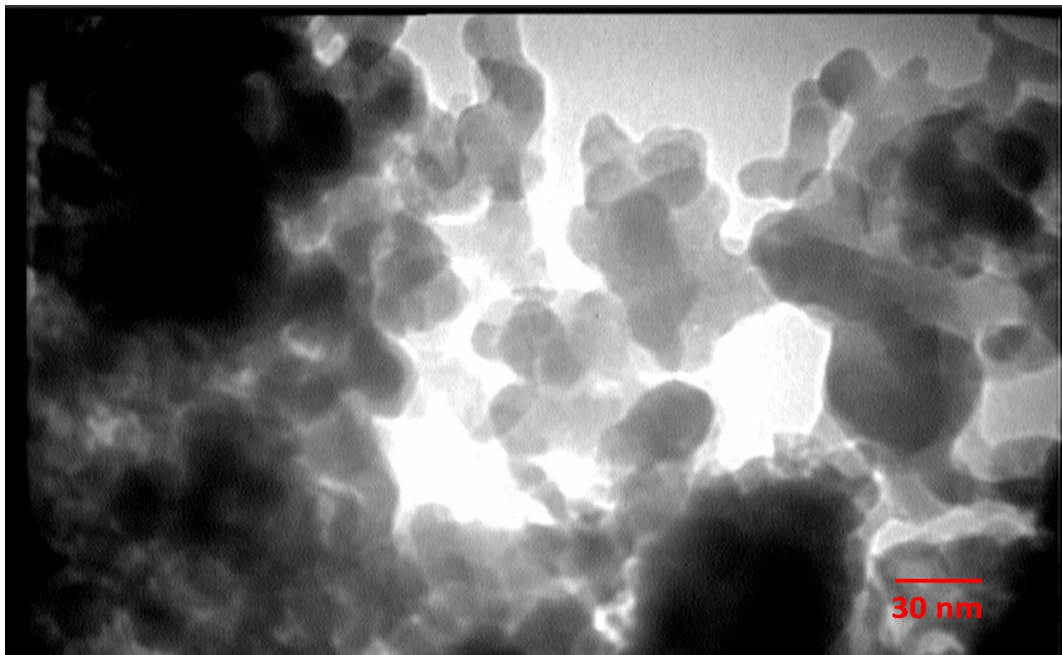
Fig. 1. TEM picture of Si_3N_4 nano-powder

Table 2. Weight percent of aluminum elements

Element	Al	Fe	Si	Mn	Cu	Mg	Ti
Concentration (wt %)	Base	0.15	0.05	0.02	0.01	0.05	0.01

The weight of all samples before and after coating process was measured and recorded by a digital scale with accuracy of 50μg. To investigate surface morphology of samples, the Zeiss Sigma and Philips XL 30 SEM were used.

Roughness test was performed on the coatings of all samples using surface roughness tester (Subtonic 25) produced by the Taylor Hobson Company. The thickness of the coatings was reported by QNix 8500 coating thickness gauge after at least 10 measurements. Corrosion behavior of samples coated by cyclic polarization method was studied using EG&G Potentiostat/ Galvanostat model 273 in 3.5 wt. %NaCl solution. The tested area of the sample surface was 0.196 cm². Cyclic polarization was performed at a potential ranging within -300 mV and +3 V versus open circuit potential (OCP) at a scan rate of 1 mV/s and scanned back to the OCP.

To determine the coefficient of friction and wear rate of coated samples, pin-on-disc wear testing was carried out in accordance with ASTM G99-95a standard and using a pin made of tungsten carbide-cobalt. In order to measure wear rate, each sample was held under wear on a circular path of radius 0.75 cm and 340 cycles and the applied normal force of 0.7 KgF.

To recognize the phases and links available in coatings, Grazing Incidence X-ray Diffraction (GIXRD) test by PANalytical X'Pert Pro MPD with step size 0.02 and radiation angle of 1° (10°- 85°; 2θ angular scan) was performed (Cu, $K_α$, λ=1.54060A˚).

3. Results and Discussion

Figure 2 presents SEM pictures of the surface coating with a uniform magnification at low current density. Porous structure, with mostly interconnected cauliflower-shaped structure porosities, is observed for all samples. Cauliflower-shaped structure decreases with the increase in additive content. This structure is also more frequently observed in coatings without additive compared to the others [19, 20]. The size and distribution of porosities on free space of coatings are almost the same.
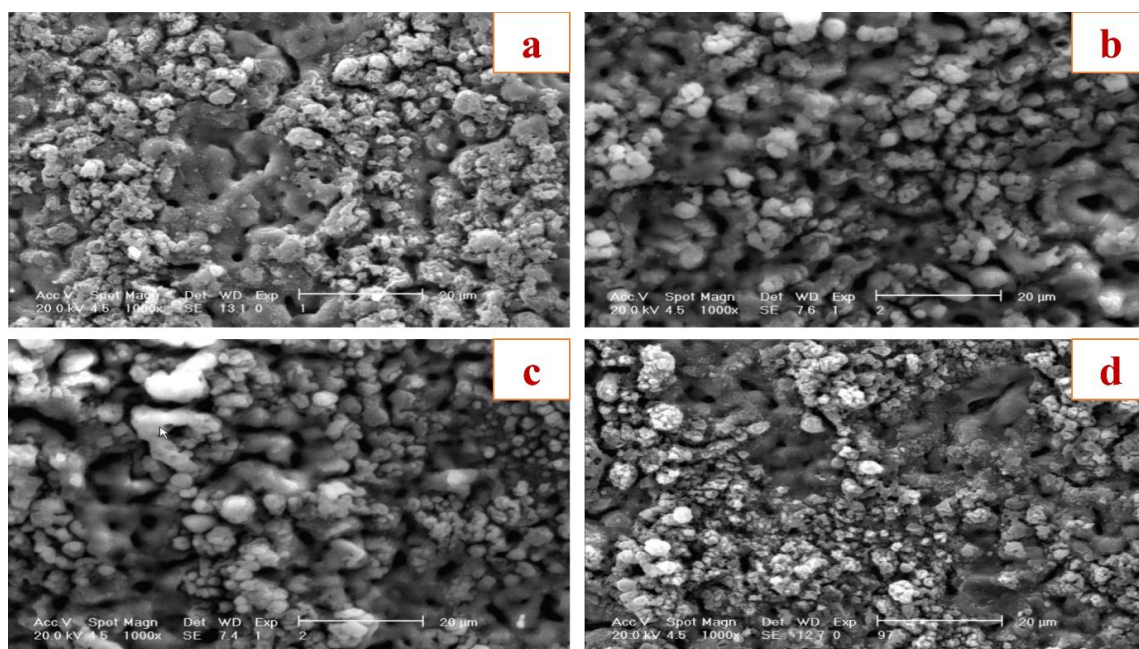
Fig. 2. SEM image of coating surface (×1000) (a) A-15-13 (b) A-15-26 (c) A-15-40 (d) P-15

Figure 3 shows SEM pictures of the surface of coated samples at higher current. Similar to the previous case, the free space structure in this case shows coatings of connected porosities that are visible under a cauliflower-shaped structure. In this case, pore size as well as cauliflower-shaped structure size is greater than similar coated samples in a current density of 15 mA/cm^2 [21]. It is observed that the pore size in all coated samples with additive has remained constant. Considering the similarity in surface structures of samples, elemental analysis of a coated surface (A-25-40) at the highest current density and concentration of additives was performed. This selection was due to the higher concentration of additives in the electrolyte and higher current density, which probably result in higher effect of electrolyte's additive [22, 23].
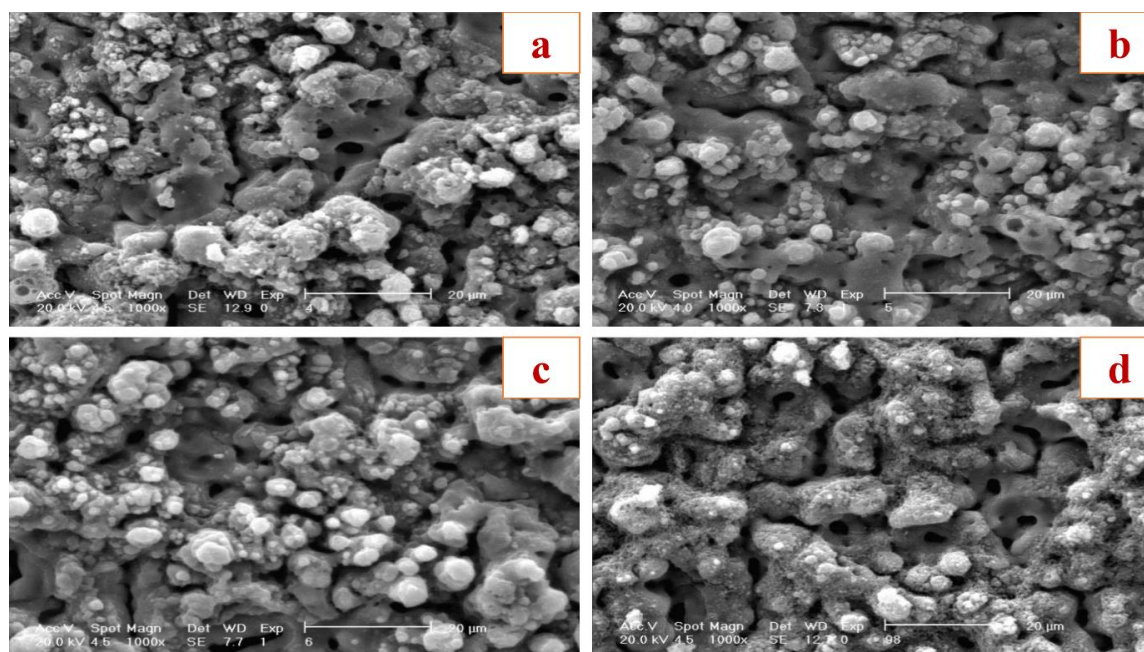

Fig. 3. SEM image of coating surface (×1000)   (a) A-25-13 (b) A-25-26 (c) A-25-40 (d) P-25

Figure 4 depicts the EDS elemental map of the mentioned surface. The results obtained from EDS elemental map shows that P-25 sample has 2.3% of N, whereas A-25-40 sample has 0.5% of N, indicating a reduction in nanoparticle by adding the additive. An explanation for this phenomenon might be that N is originally released from the Si_3N_4 nanoparticles. Here, N can be considered as a criterion for the amount of nanoparticle absorbed into the coating. The distribution of the elements shows the high presence of Si where Al content is low, and vice versa. Ni, O, and S distributions show almost a uniform process.

Figure 5 presents the SEM image of the cross section of A-25-40 sample with elemental analysis map. As shown in this Figure, aluminum-rich phases are around the intersection between coating and sub-layer, while the Si-rich phases are close to the free surface of the coating. The formed layer that was not seen apparently, can be observed clearly by the map. The studied area in Figure 5 indicates that cauliflower-shaped structure formed on the surface is rich in Ni, Si, and underside porous structure is rich in Al. The notable point is the reduction of the Ni percentage as a criterion of Nanoparticle absorption [24].
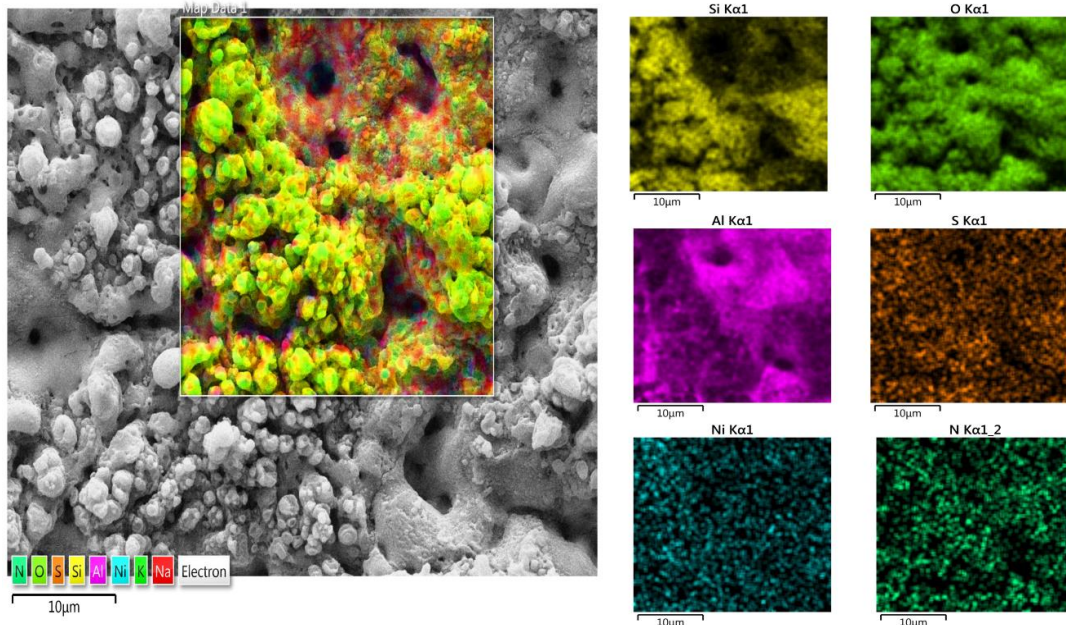

Fig. 4. SEM image of coating surface related to A-25-40 sample with elemental analysis map
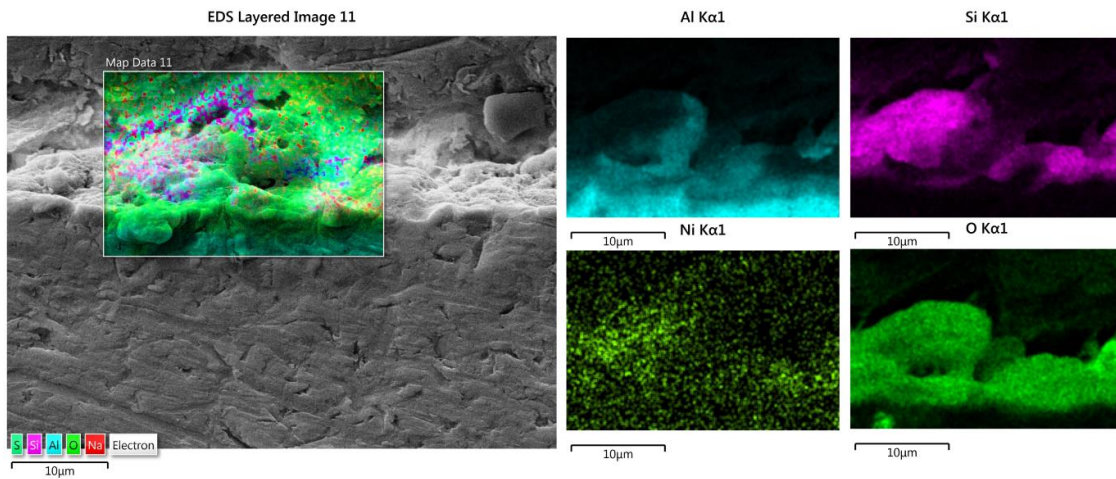

Fig. 5. SEM image of cross section related to A-25-40 sample with elemental analysis map

Figure 6 shows the TEM image of the A-25-40 sample. As shown in this figure, Si_3N_4 nanoparticles are uniformly absorbed into the coating and nanocomposite coating are successfully obtained [25]. The coating was scratched and converted in the powder from, TEM images were provided using these powders.

Figure 7 illustrates the X-Ray Diffraction pattern of the A-25-40 sample. As mentioned in this Figure, the strongest peaks are indexed to Ni_2SiO_4 (ICDD card no. 01-083-1651) and alumina (ICDD card no. 00-047-1770). Regarding the elemental analysis presented in Figure 4, it seems that cauliflower-shaped coatings are created by Si_3N_4 nano-powders, while the underside structures are created by Ni_2SiO_4 and alumina.
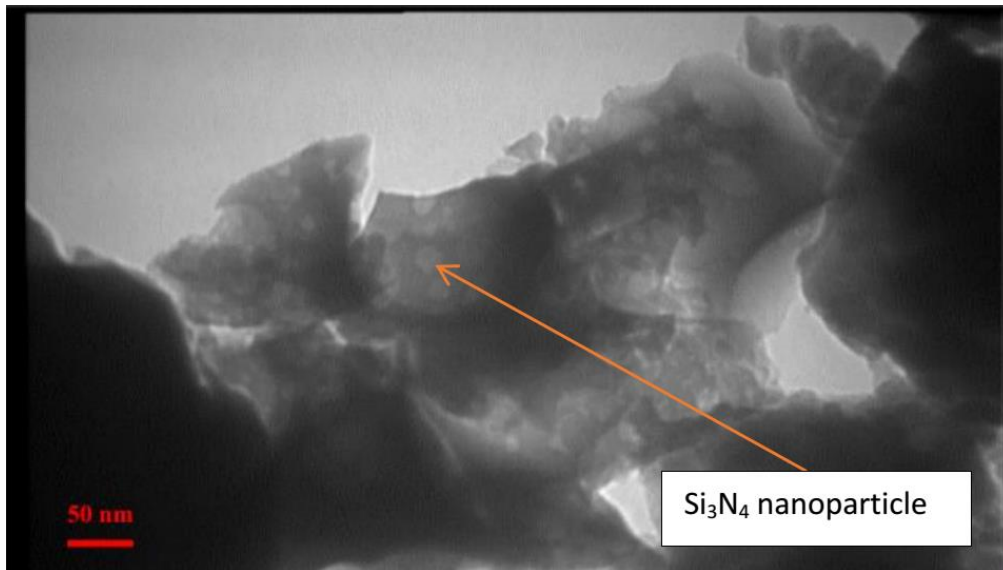

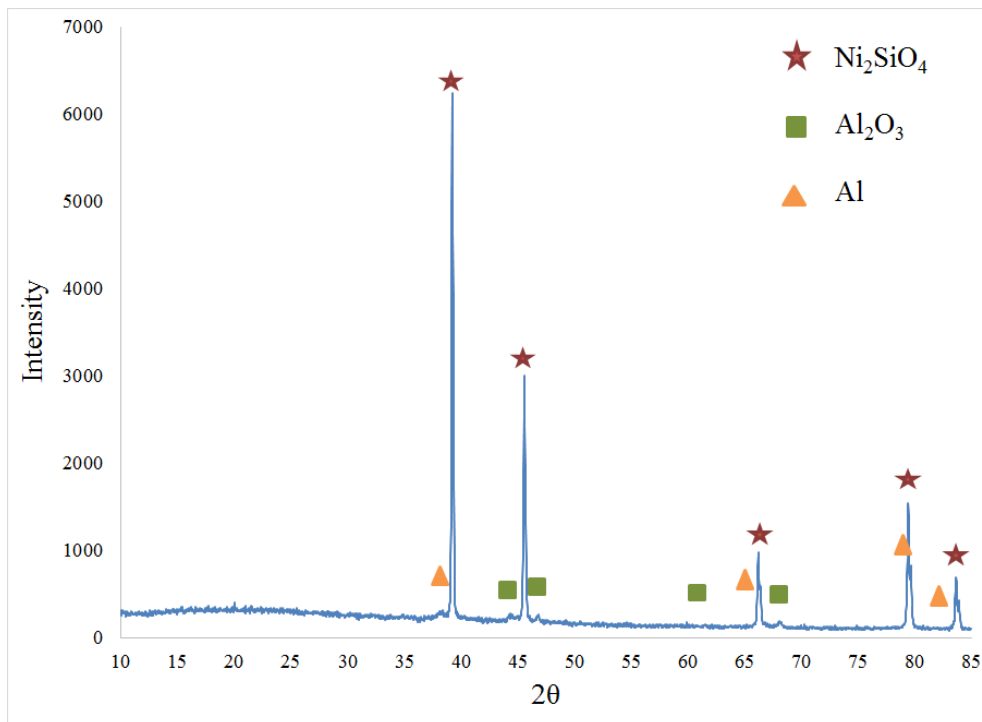**Fig. 6. TEM image related to the A-25-40 sample**

Fig. 7. Pattern of GIXRD on the A-25-40 sample

Figure 8 shows the result of measured thicknesses of various coatings, using thickness measurement gauges. At low current density, thickness changes are not so perceptible and it seems that the increase in additive density does not have considerable effect on the growth rate of coatings. On the contrary, at a current density of 25 mA/cm^2 for instance, as concentration of additive increases, thickness begins to decrease. Raising the current density with and without the presence of additive also leads to the increase in coating thickness [26, 27]. Meanwhile, the observed thickness difference between thickness measured by Thickness Gauge and SEM image of A-25-40 sample is attributed to the porous nature of these layers, which was also revealed in previous works [28].

Figure 9 shows weight changes of the coated samples. As shown, weight changes of coated samples in lower currents have remained almost constant as same as their thickness change, except A-15-13 sample. This observation might imply that the structure of the samples has not changed significantly and the additive has not influenced them extremely. At concentration of 13, this trace is not obvious, while it being sharp at higher concentrations. Besides, at higher currents, although their thickness is lower than that of the samples without additive, their weight change is greater probably because of a denser coating. This observation in A-25-13 and A-25-26 samples is sharper than A-25-26 and A-25-40 samples. At higher currents, it seems that the additive has the highest effect on the coating mechanism [29, 30].
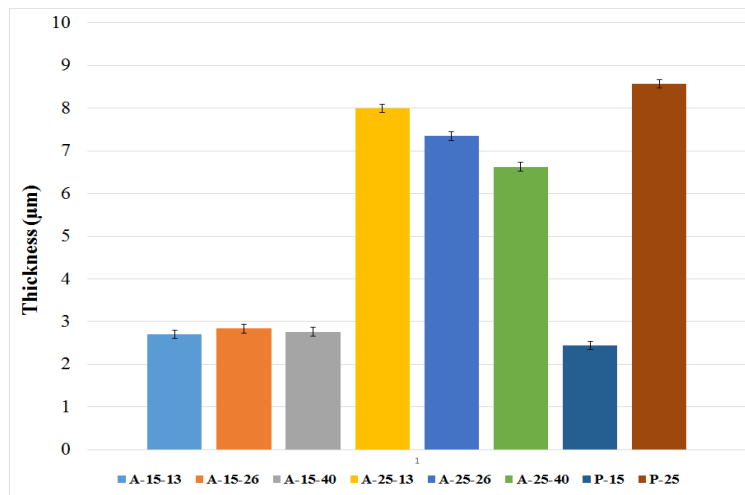

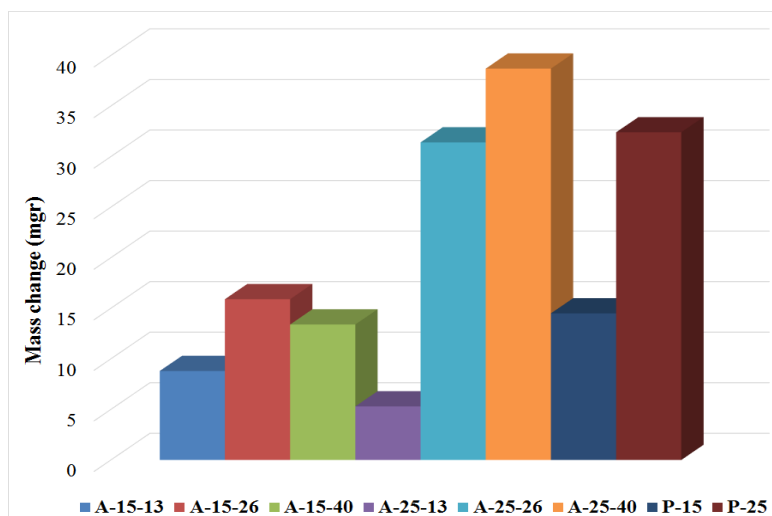**Fig. 8. Results of the thickness measurement of coated samples**

Fig. 9. Graph of the weight changes in samples before and after the coating

Figure 10 illustrates the cyclic polarization curve of each sample after 24 hours of immersion in 3.5% NaCl solution. As it demonstrates, current of anodic branches in samples with additive is less than that of those without additive. Table 3 presents the results obtained from the cyclic polarization curve. Polarization resistance (R_p) is calculated by solving the Stern–Geary equation expressed as follow [31-33]:

$$R_p = \frac{\beta_a \beta_c}{2.3 i_{corr} (\beta_a + \beta_c)}$$

where i_{corr}, β_a and β_c are corrosion current density, anodic Tafel slope, and cathodic Tafel slope, respectively. As shown in Table 3, corrosion potential approximately remained constant. However, Figure 10 shows that the direct current of anodic branch at potentials higher than -400 mV was considerably lower in the samples with additive as compared to the samples without any additive. Nevertheless, reverse-current of anodic branch varies significantly among the samples. Table 3 shows current values at the highest potential and area under the curve as a criterion of direct and reverse currents of the anodic path, respectively [34, 35].
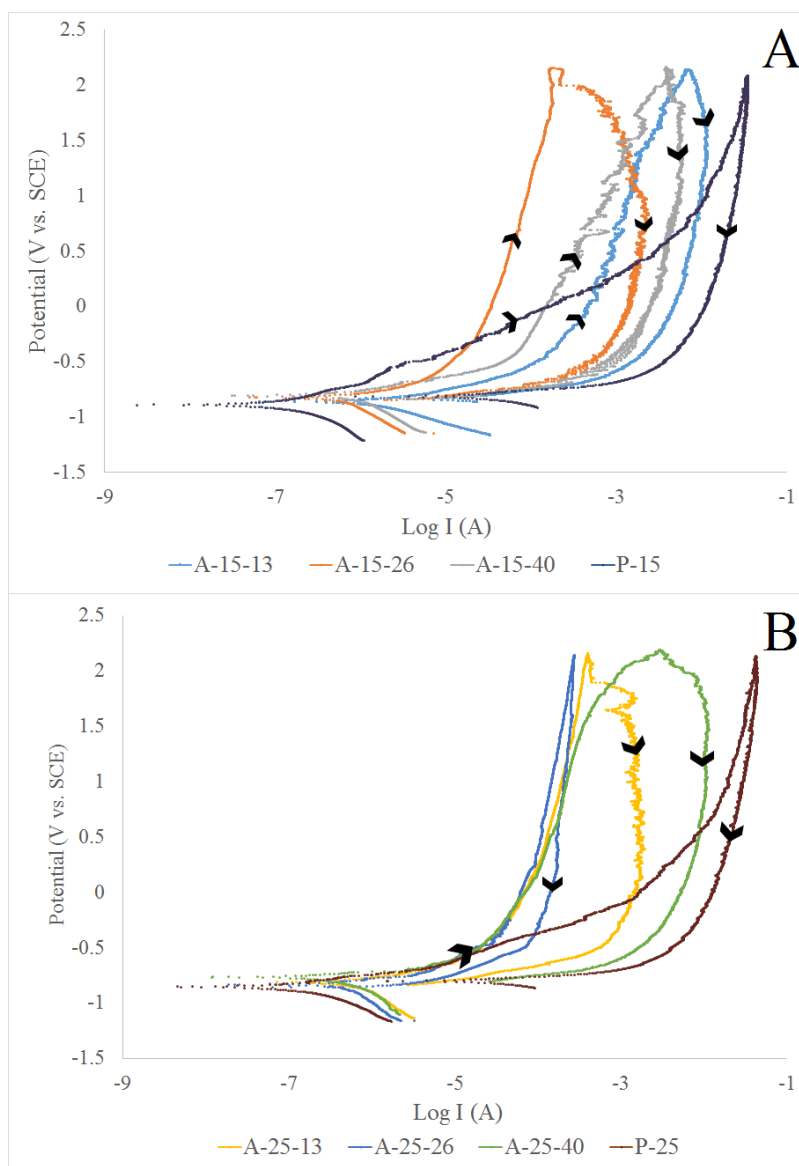

Fig. 10. Cyclic Potentiodynamic polarization curves of different treated samples after 24 hours of immersion in 3.5% NaCl solution

140

Table 3. Results extracted from the cyclic polarization curve of coated samples

sample	E_{corr} (mV vs. SCE)	I_{corr} (μA)	I in E_{max} (μA)	Internal Surface (V.Log I)	(mV/decade)β_c	β_a (mV/decade)	R_p ($10^3 \Omega$)
A-15-13	-859	1.553	6390	2.520	240	135	24.18
A-15-26	-830	0.5013	168	3.871	302	148	86.14
A-15-40	-805	0.5052	3830	2.883	215	146	74.83
A-25-13	-820	0.5284	398	2.816	276	132	73.47
A-25-26	-824	0.4161	273	0.346	427	85	74.07
A-25-40	-763	0.2532	2890	5.553	230	109	126.98
p-15	-868	0.1427	35200	3.443	320	219	396.14
p-25	-851	0.4609	9430	2.500	299	146	92.53

Reverse branch of all samples had positive hysteresis meaning that pits could not retrieve themselves, except the A-25-26 sample that had the lowest direct-current and in the reverse path, despite other samples reversed close to the direct path. As presented in Table 3 (I in E_{max} column), adding $NiSO_4$ to electrolyte results in higher resistance to pitting in coatings. Besides, it shows that R_p value for A-25-40 sample is greater than that of the other samples, although the anodic behavior of the A-25-26 sample is better. Since these coatings are susceptible to pitting corrosion, the behavior of the anodic branch is more important [36, 37]. Corrosion currents of these samples and P-25 sample are almost equal.

Figure 11 shows the results of wear testing performed on coated samples as well as changes in coefficient of friction. Results of wear and roughness tests are also demonstrated in Table 4. The changes in the concentration of additive at high and low currents do not lead to a considerable change in the roughness of samples. However, roughness is slightly increased compared to the samples without additive. The average measured coefficient of friction for all samples fallows a fixed route, but it reduces once the additive becomes approximately the half [38, 39].

The noteworthy point in Table 4 is the increase in the wear rate of samples with additive compared to those without additive. The presented results of the wear rate of samples are for four wear tests (Fig. 12), where their average is reported. Clearly, at low currents, despite an appropriate corrosion behavior, the wear rate is increased and samples do not have the same behavior during these four steps. In comparison, at high currents, wear rate is tracked the wear rate of samples without additive by rubbing the outer layer that shows high impact of additive on the surface of coatings. On the other hand, absorbing nanoparticles in coating is reduced by adding the additive. Increase in wear rate can be due to the low-level presence of nanoparticle. Therefore, it can be stated that although addition of additive probably reduces the coefficient of friction, it causes a lower nanoparticle absorption, leading to an increase in wear rate compared to the samples without additive.

4. Conclusion

Plasma electrolytic oxidation (PEO) was performed on a 1010 aluminum alloy using direct current. To obtain a nanocomposite structure, Si_3N_4 nanoparticles were added into the electrolyte. In alkaline aqueous suspension (silicate-based), the effect of $NiSO_4$ additions was investigated. Observing the SEM image, elemental analysis, and XRD results, it was found that by adding additive, Ni_2SiO_4 phase is formed in the coating and the obtained coatings are denser. In addition, since corrosion behavior of coatings with additive is also improved, for samples with current density of 15 mA/cm^2 anodic branch current decreases between 1 and 2 decades, while for samples with current density of 25 mA/cm^2, this reduced amount at the highest potential is between 0.7 and 1 decades. Roughness of samples with the additive also increased with a range of 8 to 3%. However, coefficient of friction was reduced approximately by half. Wear rate of samples with additive also probably increased due to the reduction of nanoparticle absorption into the coating.
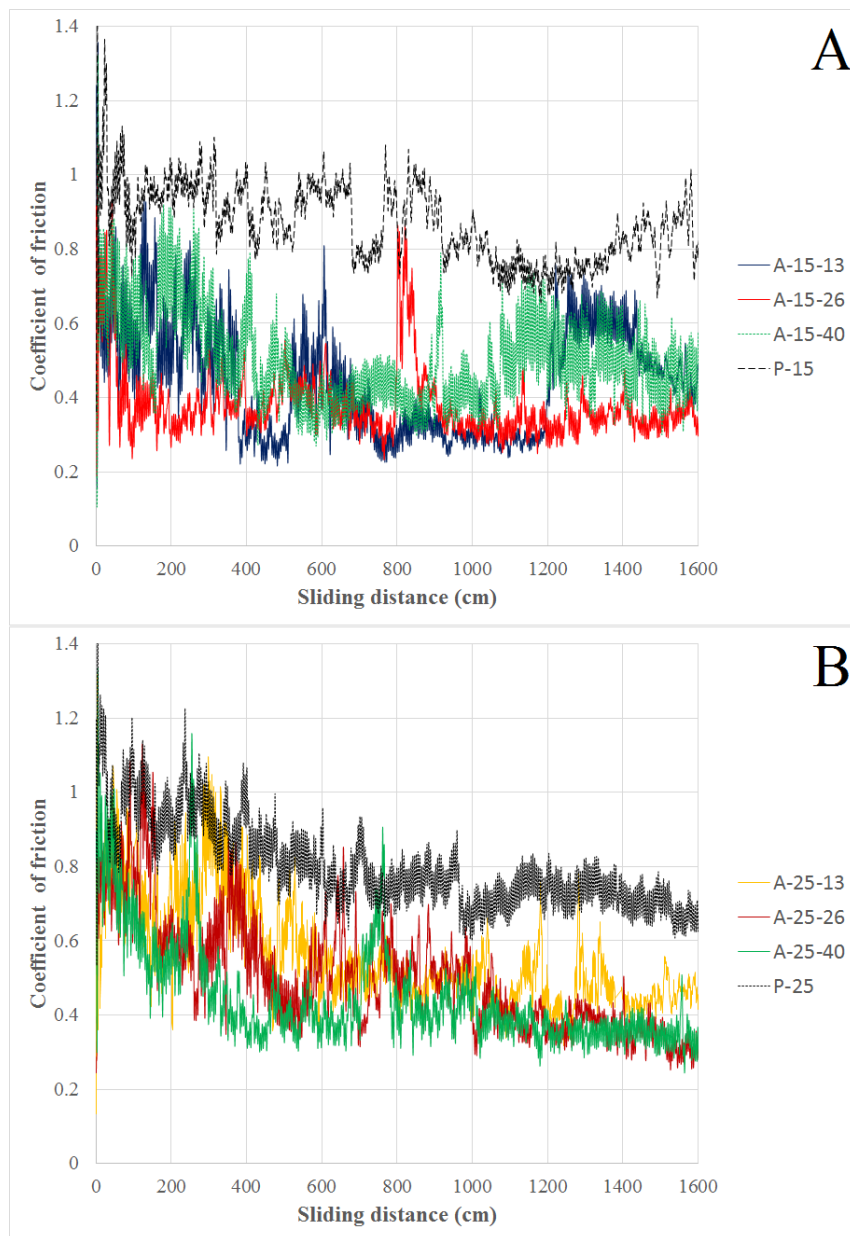
Fig. 11. Coefficient of friction changes curve based on eroded distance for samples coated with current density of (A) 15 mA/cm^2 (B) 25 mA/cm^2

Table 4. Average of coefficient of friction, wear rate and surface roughness of coated samples

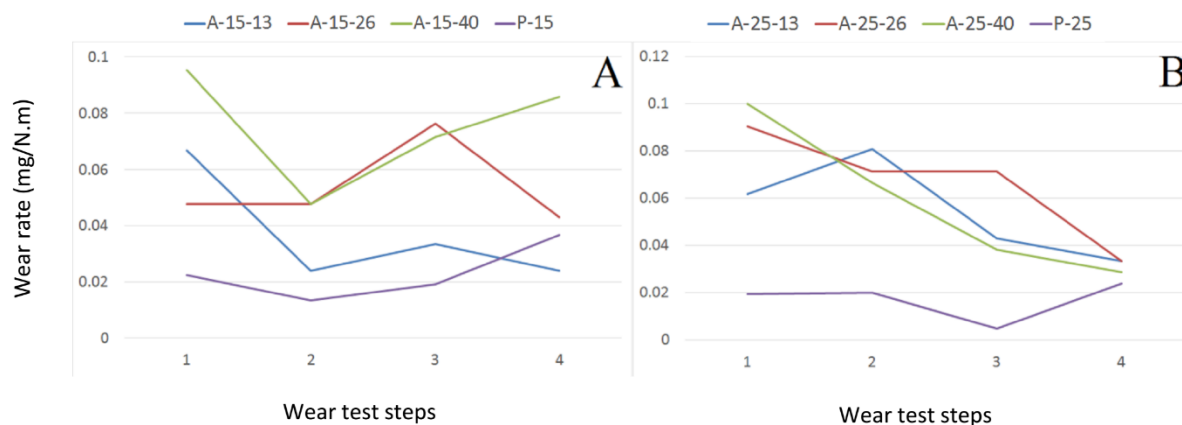| Sample	Average of coefficient of friction	Wear rate (mg/N.m)	R$_a$ (μm)
A-15-13	0.446	0.036	0.96
A-15-26	0.38	0.053	0.739
A-15-40	0.499	0.075	0.796
A-25-13	0.561	0.054	1.58
A-25-26	0.5	0.066	1.62
A-25-40	0.448	0.058	1.62
p-15	0.866	0.021	0.62
p-25	0.8	0.017	1.45

Fig. 12. Wear rate at each step of wear testing for (A) 15 mA/cm^2 (B) 25 mA/cm^2 samples

References

[1]. T. Wei, F. Yan, J. Tian, Journal of Alloys and Compounds, Vol. 389 (2005) pp. 169-176.

[2]. M. Treviño, R.D. Mercado-Solis, R. Colás, A. Pérez, J. Talamantes, A. Velasco, Wear, Vol. 301 (2013) pp. 434-441.

[3]. J. Tian, Z. Luo, S. Qi, X. Sun, Surface and Coatings Technology, Vol. 154 (2002) pp. 1-7.

[4]. Y.-J. Oh, J.-I. Mun, J.-H. Kim, Surface and Coatings Technology, Vol. 204 (2009) pp. 141-148.

[5]. G. Thompson, H. Habazaki, K. Shimizu, M. Sakairi, P. Skeldon, X. Zhou, G. Wood, Aircraft Engineering and Aerospace Technology, Vol. 71 (1999) pp. 228-238.

[6]. X. Sun, Z. Jiang, S. Xin, Z. Yao, Thin Solid Films, Vol. 471 (2005) pp. 194-199.

[7]. M. Tang, W. Li, H. Liu, L. Zhu, Current Applied Physics, Vol. 12 (2012) pp. 1259-1265.

[8]. G. Sundararajan, L. Rama Krishna, Surface and Coatings Technology, Vol. 167 (2003) pp. 269-277.

[9]. S. Stojadinovic, R. Vasilic, I. Belca, M. Petkovic, B. Kasalica, Z. Nedic, L. Zekovic, Corrosion Science, Vol. 52 (2010) pp. 3258-3265.

[10]. D. Sreekanth, N. Rameshbabu, K. Venkateswarlu, C. Subrahmanyam, L. Rama Krishna, K. Prasad Rao, Surface and Coatings Technology, Vol. 222 (2013) pp. 31-37.

[11]. D. Sreekanth, N. Rameshbabu, K. Venkateswarlu, Ceramics International, Vol. 38 (2012) pp. 4607-4615.

[12]. L.O. Snizhko, A.L. Yerokhin, A. Pilkington, N.L. Gurevina, D.O. Misnyankin, A. Leyland, A. Matthews, Electrochimica Acta, Vol. 49 (2004) pp. 2085-2095.

[13]. D.-J. Shen, Y.-L. Wang, P. Nash, G.-Z. Xing, Journal of Materials Processing Technology, Vol. 205 (2008) pp. 477-481.

[14]. D. Shen, G. Li, C. Guo, J. Zou, J. Cai, D. He, H. Ma, F. Liu, Applied Surface Science, Vol. 287 (2013) pp. 451-456.

[15]. M. Petković, S. Stojadinović, R. Vasilić, I. Belča, Z. Nedić, B. Kasalica, U.B. Mioč, Applied Surface Science, Vol. 257 (2011) pp. 9555-9561.

[16]. J. Li, Z. Shao, X. Zhang, Y. Tian, Surface and Coatings Technology, Vol. 200 (2006) pp. 3010-3015.

[17]. M. Aliofkhazraei, A.S. Rouhaghdam, Nanocomposite coatings, Nova Science Publishers, 2011.

[18]. M. Aliofkhazraei, A. Sabour Rouhaghdam, Surface and Coatings Technology, Vol. 205 (2010) pp. 51-56.

[19]. M. Aliofkhazraei, A. Sabour Rouhaghdam, Fabrication of Nanostructures by Plasma Electrolysis, John Wiley Publisher, 2010.

[20]. M. Aliofkhazraei, P. Taheri, A. Sabour Rouhaghdam, C. Dehghanian, Materials Science, Vol. 43 (2007) pp. 791-799.

[21]. A.L. Yerokhin, X. Nie, A. Leyland, A. Matthews, S.J. Dowey, Surface and Coatings Technology, Vol. 122 (1999) pp. 73-93.

[22]. S.V. Gnedenkov, V.S. Egorkin, S.L. Sinebryukhov, I.E. Vyaliy, A.S. Pashinin, A.M. Emelyanenko, L.B. Boinovich, Surface and

Coatings Technology, Vol. 232 (2013) pp. 240-246.

[23]. V. Dehnavi, B.L. Luan, D.W. Shoesmith, X.Y. Liu, S. Rohani, Surface and Coatings Technology, Vol. 226 (2013) pp. 100-107.

[24]. M. Aliofkhazraei, A. Sabour Rouhaghdam, T. Shahrabi, Surface and Coatings Technology, Vol. 205, Supplement 1 (2010) pp. 41-46.

[25]. M. Aliofkhazraei, A.S. Rouhaghdam, E. Ghobadi, Journal of Nanoscience and Nanotechnology, Vol. 11 (2011) pp. 9057-9060.

[26]. Y.Q. Zhou, C. Gao, X.C. Shi, J.Y. Xu, X. Jiang, Advanced Materials Research, Vols. 1030-1032, 2014, pp. 165-169.

[27]. K. Wang, B.H. Koo, C.G. Lee, Y.J. Kim, S. Lee, E. Byon, Chinese Journal of Aeronautics, Vol. 22 (2009) pp. 564-568.

[28]. H.R. Masiha, H.R. Bagheri, M. Gheytani, M. Aliofkhazraei, A. Sabour Rouhaghdam, T. Shahrabi, Applied Surface Science, Vol. 317 (2014) pp. 962-969.

[29]. L. Wang, L. Chen, Z. Yan, H. Wang, J. Peng, Journal of Alloys and Compounds, Vol. 480 (2009) pp. 469-474.

[30]. D. Wu, X. Liu, K. Lu, Y. Zhang, H. Wang, Applied Surface Science, Vol. 255 (2009) pp. 7115-7120.

[31]. B. Yoo, K.R. Shin, D.Y. Hwang, D.H. Lee, D.H. Shin, Applied Surface Science, Vol. 256 (2010) pp. 6667-6672.

[32]. S. Feliu, C. Maffiotte, A. Samaniego, J.C. Galván, V. Barranco, Applied Surface Science, Vol. 257 (2011) pp. 8558-8568.

[33]. V. Shinde, A.B. Gaikwad, P.P. Patil, Applied Surface Science, Vol. 253 (2006) pp. 1037-1045.

[34]. L. Wang, L. Chen, H.L. Wang, Z.C. Yan, J.Z. Peng, Corrosion and Protection, Vol. 30 (2009) pp. 388-391.

[35]. X. Nie, X. Li, D. Northwood, Materials Science Forum, Vols. 546-549, 2007, pp. 1093-1100.

[36]. U. Trdan, J. Grum, Corrosion Science, Vol. 59 (2012) pp. 324-333.

[37]. A.S. Hamdy, F. Alfosail, Z. Gasem, Electrochimica Acta, Vol. 89 (2013) pp. 749-755.

[38]. M. Aliofkhazraei, A.S. Rouhaghdam, Surface and Coatings Technology, Vol. 205, Supplement 2 (2011) pp. 57-62.

[39]. Y. Cheng, J. Cao, Z. Peng, Q. Wang, E. Matykina, P. Skeldon, G.E. Thompson, Electrochimica Acta, Vol. 116 (2014) pp. 453-466.